Article

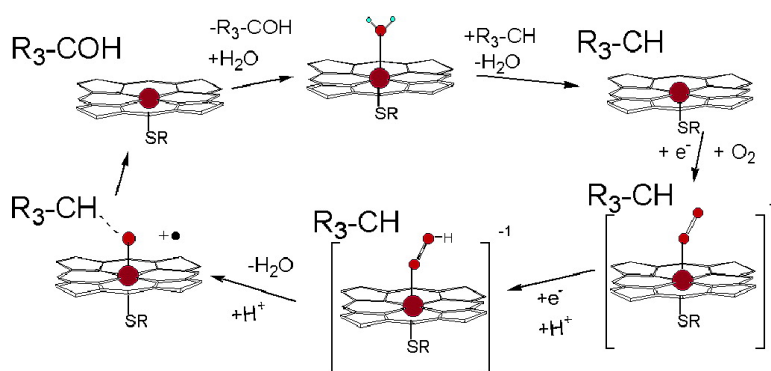# Cytochrome P450CAM Enzymatic Catalysis Cycle: A Quantum Mechanics/Molecular Mechanics Study

Victor Guallar, and Richard A. Friesner

More About This Article

Additional resources and features associated with this article are available within the HTML version:

- Supporting Information
- Links to the 9 articles that cite this article, as of the time of this article download
- Access to high resolution figures
- Links to articles and content related to this article
- Copyright permission to reproduce figures and/or text from this article

View the Full Text HTML

Cytochrome P450CAM Enzymatic Catalysis Cycle: A Quantum Mechanics/Molecular Mechanics Study

Victor Guallar[†] and Richard A. Friesner*

Contribution from the Department of Chemistry and Center for Biomolecular Simulations, Columbia University, New York, New York 10027

Received May 13, 2003; E-mail: rich@chem.columbia.edu

Abstract: The catalytic pathway of cytochrome P450cam is studied by means of a hybrid quantum mechanics/molecular mechanics method. Our results reveal an active role of the enzyme in the different catalytic steps. The protein initially controls the energy gap between the high- and low-spin states in the substrate binding process, allowing thermodynamic reduction by putidaredoxin reductase and molecular oxygen addition. A second electron reduction activates the delivery of protons to the active site through a selective interaction of Thr252 and the distal oxygen causing the O−O cleavage. Finally, the protein environment catalyzes the substrate hydrogen atom abstraction step with a remarkably low free energy barrier (∼8 kcal/mol). Our results are consistent with the effect of mutations on the enzymatic efficacy and provide a satisfactory explanation for the experimental failure to trap the proposed catalytically competent species, a ferryl Fe(IV) heme.

Introduction

Among heme proteins, the cytochrome P450 monooxygenase family plays a vital role in the metabolism of xenobiotic substances in plants, fungi, bacteria, insects, and mammals.[1−3] In mammals, for example, hydroxylation metabolites of polycyclic aromatic hydrocarbons have long been of interest to researchers because of their relevance to chemical carcinogenesis.[4−6] Many of the detailed studies of P450 have focused on the bacterial P450cam (for which camphor is the substrate), the first soluble P450 protein to have its sequence and X-ray structure determined.[7] The complex pathway from the inactive resting species to the putative catalytically active ferryl species (compound I) is believed to be common across different P450 members and involves sequential changes in oxidation state, ligand composition, and spin state of the heme.[8−16] In the consensus mechanism, shown in Figure 1, following the initial

substrate binding and displacement of a loosely bound water ligand, one-electron reduction of the iron occurs, after which molecular oxygen binds forming the last quasi-stable P450 intermediate.[17,18] Subsequent formation of the supposed catalytically active compound I requires a second reduction and the addition of two protons.[19] There is substantial indirect evidence[13,16] that the hydroxylation mechanism proceeds via abstraction of a hydrogen from the camphor substrate, analogous to that operative in methane monooxygenase (MMO).[9] However, there is little direct experimental data concerning the ferric superoxide reduction and protonation mechanism, steps **3→5** in Figure 1 (throughout the text, the bold numbers refer to species in Figure 1), and the substrate hydroxylation, steps **5→6** in Figure 1. These aspects of the catalytic cycle have been the principal focus of our effort.

In this paper, an exhaustive theoretical study of the hydroxylation catalytic pathway of cytochrome P450cam is obtained by means of a mixed quantum mechanics/molecular mechanics (QM/MM) technique. The paper is organized in the following manner. We first give a brief overview of the various steps in the catalytic cycle, emphasizing recent experimental data as well as relevant computational studies. In the Computational Methods, the QM/MM systems and the protocols employed are introduced. The Results section is then presented. In the

---

[†] Present address: Department of Biochemistry and Molecular Biophysics, Washington University, St. Louis, MO 63108.

(1) Porter, T. D.; Coon, M. J. *J. Biol. Chem.* **1991**, *266* (21), 13469−13472.
(2) *Cytochrome P450: Structure, Mechanism and Biochemistry*, 2nd ed. Plenum: New York, 1995.
(3) Guengerich, F. P. *J. Biol. Chem.* **1991**, *266* (16), 10019−10022.
(4) Hayes, C. L.; Spink, D. C.; Spink, B. C.; Cao, J. Q.; Walker, N. J.; Sutter, T. R. *Proc. Natl. Acad. Sci. U.S.A.* **1996**, *93* (18), 9776−9781.
(5) Mckay, J. A.; Melvin, W. T.; Ahsee, A. K.; Ewen, S. W. B.; Greenlee, W. F.; Marcus, C. B.; Burke, M. D.; Murray, G. I. *Febs Lett.* **1995**, *374* (2), 270−272.
(6) Savas, U.; Christou, M.; Jefcoate, C. R. *Carcinogenesis* **1993**, *14* (10), 2013−2018.
(7) Poulos, T. L.; Finzel, B. C.; Howard, A. J. *J. Mol. Biol.* **1987**, *195* (3), 687−700.
(8) De Visser, S. P.; Ogliaro, F.; Harris, N.; Shaik, S. *J. Am. Chem. Soc.* **2001**, *123* (13), 3037−3047.
(9) Guallar, V.; Gherman, B. F.; Miller, W. H.; Lippard, S. J.; Friesner, R. A. *J. Am. Chem. Soc.* **2002**, *124*, 3377−3384.
(10) Loew, G. H.; Harris, D. L. *Chem. Rev.* **2000**, *100* (2), 407−419.
(11) Schlichting, I.; Berendzen, J.; Chu, K.; Stock, A. M.; Maves, S. A.; Benson, D. E.; Sweet, B. M.; Ringe, D.; Petsko, G. A.; Sligar, S. G. *Science* **2000**, *287* (5458), 1615−1622.
(12) Harris, D.; Loew, G. H. *Biophys. J.* **1994**, *66* (2), A137.

(13) Davydov, R.; Makris, T. M.; Kofman, V.; Werst, D. E.; Sligar, S. G.; Hoffman, B. M. *J. Am. Chem. Soc.* **2001**, *123* (7), 1403−1415.
(14) Ogliaro, F.; De Visser, S. P.; Shaik, S. *J. Inorg. Biochem.* **2001**, *86* (1), 363.
(15) Davydov, R.; Macdonald, I. D. G.; Makris, T. M.; Sligar, S. G.; Hoffman, B. M. *J. Am. Chem. Soc.* **1999**, *121* (45), 10654−10655.
(16) Ogliaro, F.; Harris, N.; Cohen, S.; Filatov, M.; De Visser, S. P.; Shaik, S. *J. Am. Chem. Soc.* **2000**, *122* (37), 8977−8989.
(17) Egawa, T.; Ogura, T.; Makino, R.; Ishimura, Y.; Kitagawa, T. *J. Biol. Chem.* **1991**, *266* (16), 10246−10248.
(18) Bangcharoenpaurpong, O.; Rizos, A. K.; Champion, P. M.; Jollie, D.; Sligar, S. G. *J. Biol. Chem.* **1986**, *261* (18), 8089−8092.
(19) Aikens, J.; Sligar, S. G. *J. Am. Chem. Soc.* **1994**, *116* (3), 1143−1144.
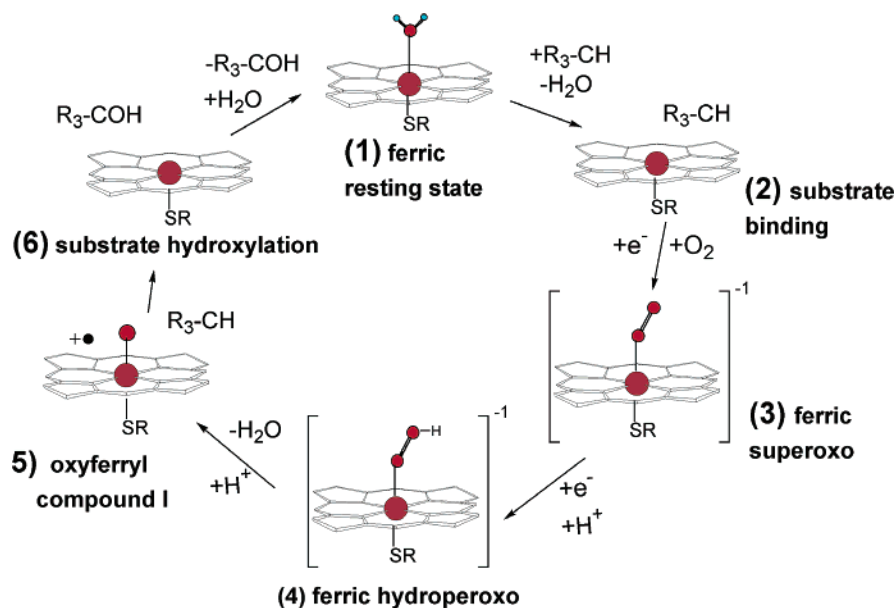
Figure 1. Catalytic cycle common in most cytochrome P450s. (1) Ferric resting state. (2) Substrate binding displaces coordinated water. (3) Ferric superoxide: first reduction results in O₂ binding. (4) Second reduction and distal oxygen protonation with the proposed ferric hydroperoxo. (5) Second protonation, O−O cleavage producing a water molecule and the active oxyferryl compound I. (6) Substrate hydroxylation and resting state regeneration by water coordination.

Discussion, we analyze the results to obtain physical insight from the calculations. Finally, the Conclusion summarizes what we have learned and briefly discusses future directions. Throughout the Results and the Discussion, we follow the same enzymatic cycle scheme used in the Introduction, steps **1→2**, **3→5**, and **5→6**.

Overview of Catalytic Cycle. Substrate Binding. Steps 1→2. The first question in the catalytic pathway is the origin of the low-spin resting state, which is unusual in a ferric aquo heme complex.[20] The main controversy is in the role of the protein in modulating the spin state, a property of the heme unit that is central to the maintenance of the enzymatic function. Semiempirical INDO calculations support an active role of the protein.[21] More recently, however, such an unusual low-spin state has been explained by means of a more accurate (larger basis set) description of the thiolate axial ligand.[22] This last result, obtained using a reduced model for the heme active site, reproduces the low-spin state without the need of the protein environment.

The first catalytic step from the low-spin resting state involves camphor binding, which displaces the water molecule from the heme pocket. This binding produces a shift from low-to-high spin, accompanied by a 130-mV increase in the reduction potential, which allows thermodynamic reduction by putidaredoxin reductase. After this one-electron reduction, molecular oxygen binds, forming the last quasi-stable P450 intermediate. The crystal structure of the ferric superoxo in P450cam has recently been obtained by means of cryogenic temperatures and rapid data collection techniques.[11]

Ferric Superoxo Protonation and O−O Bond Cleavage. Steps 3→5. The stepwise transformation of the ferric superoxide to compound I, involving a reduction and an addition of two protons, is sufficiently rapid to have eluded direct experimental characterization. Recently, a resonance Raman and EPR experi-

ment on P450cam[23] and a theoretical study on P450eryf[24] indicated the need for reduction prior to proton addition. Cryogenic crystallographic studies[11] have indicated the presence of a water, W901, and a threonine OH group, Thr252, in hydrogen-bonded distance to the dioxygen heme ligand in the ferric superoxide species. Isotopic labeling studies have revealed that the proximal oxygen, directly bound to the heme iron, is transferred to substrates, while the distal oxygen is involved in the concurrent formation of water.[25,26] These results suggest a selective distal oxygen protonation mechanism. The crystal structure also reveals the existence of a water channel linking Thr252 and Glu366, which is stable throughout molecular dynamics simulations.[27] Davydov et al.,[13] using EPR spectra and ENDOR techniques, pointed to a hydroperoxo-ferric-intermediate (**4** in Figure 1) as the species trapped in cryogenic conditions (77 K). Thus even at this temperature one proton can be delivered upon reduction of the ferric superoxo. The same study investigated the importance of Thr252. Mutation of Thr252 to Ala (T252A) did not yield any product, but a signal for the hydroperoxo intermediate **4** was still obtained. This results suggests that **4** is a key intermediate close to the branch-point leading either to product formation or to uncoupling and hydrogen peroxide production. Previous experimental results,[28] with a methoxy group in place of the Thr252 hydroxy group, showed a retention of the monooxygenase activity although with a considerable decrease of O₂ consumption rate. Thus, the role of Thr252 as an acid catalyst has been reconsidered, and

(20) Lipscomb, J. D. *Biochemistry* **1980**, *19* (15), 3590−3599.
(21) Harris, D.; Loew, G. *J. Am. Chem. Soc.* **1993**, *115* (19), 8775−8779.
(22) Green, M. T. *J. Am. Chem. Soc.* **1998**, *120* (41), 10772−10773.

(23) Sjodin, T.; Christian, J. F.; Macdonald, I. D. G.; Davydov, R.; Unno, M.; Sligar, S. C.; Hoffman, B. M.; Champion, P. M. *Biochemistry* **2001**, *40* (23), 6852−6859.
(24) Guallar, V.; Harris, D. L.; Batista, V. S.; Miller, W. H. *J. Am. Chem. Soc.* **2002**, *124* (7), 1430−1437.
(25) Jones, J. P.; Rettie, A. E.; Trager, W. F. *J. Med. Chem.* **1990**, *33* (4), 1242−1246.
(26) Atkins, W. M.; Sligar, S. G. *Biochemistry* **1988**, *27* (5), 1610−1616.
(27) Harris, D. L.; Loew, G. H. *J. Am. Chem. Soc.* **1994**, *116* (26), 11671−11674.
(28) Kimata, Y.; Shimada, H.; Hirose, T.; Ishimura, Y. *Biochem. Biophys. Res. Commun.* **1995**, *208* (1), 96−102.

alternative paths linking Asp251 with the active site have been proposed.[29,30]

Substrate Hydroxylation. Steps 5→6. The cryogenic crystal study also yielded a crystallographic structure initially assigned to compound I, the oxyferryl catalytically active intermediate. In addition to the X-ray results,[11] there is evidence, from transient spectral[31] and isotopic studies,[25] of the involvement of an Fe−O bound species in the monooxygenase reaction. There is, therefore, substantial *indirect* evidence that the hydroxylation reaction proceeds via abstraction of a hydrogen by **5** from the camphor substrate. Furthermore, this mechanism is analogous to that operative in methane monooxygenase (MMO), in which a similar hydrogen atom abstraction is carried out via a non-heme diiron species, with the iron atoms in the Fe(IV) oxidation state as in compound I. Recent computational studies of the MMO reaction by our group and others are in excellent agreement with the experimental data and confirm that a classical radical abstraction transition state, followed by the formation of a bound radical intermediate (competing with a concerted channel bypassing this intermediate), is the only plausible pathway for hydroxylation to occur. In the present case, it is similarly difficult to suggest a sterically and energetically reasonable alternative. When the hydroxylation dynamics are studied, the EPR and ENDOR experiments[13] fail to obtain a signal corresponding to an Fe(IV) ferryl species, as would be expected for compound I. The ENDOR data show that the first detectable intermediate after **5** is a hydroxycamphor Fe(III) bound species. Moreover, the camphor proton whose bond is broken during hydroxylation appears to be trapped in such an intermediate. These observations indicate that the reactive hydroxylating species in P450cam is indeed the high-valent intermediate compound I. There is, however, no direct observation of this intermediate.

The most straightforward explanation of the failure to observe a ferryl intermediate in the cytochrome P450 catalytic cycle is that the barrier to hydrogen atom abstraction is sufficiently low to enable rapid interconversion of this intermediate to a hydroxylated species. Previous theoretical studies have reported high barriers and large endothermic reactions associated with reduced model studies of the hydroxylation process. The activation energy obtained in these calculations was larger than 20 kcal/mol, far too large to explain the experimental results, even when adding a zero-point correction comparable to that calculated for MMO. Theoretical calculations[16] have proposed the existence of a quartet−doublet two-state mechanism, the hydrogen abstraction activation barrier being the same for both states. By using larger reduced models, Yoshizawa et al.[29] has questioned the two-state mechanism, obtaining a lower hydrogen atom abstraction barrier for the quartet spin state. Kinetic isotope effect studies by Newcomb et al.[32] have recently reported evidence of a two-oxidant model in contrast to the two-state model.

Computational Methods

The complicated reaction at the metal center that includes bond formation and cleavage, as well as electron transfer, mandates a quantum chemical treatment of the active site. On the other hand, the
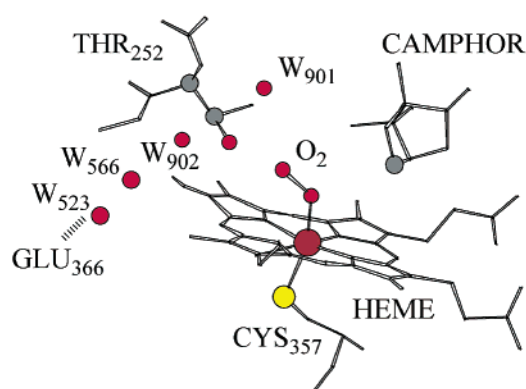

Figure 2. Active site for the ferric superoxo species. Water 902, 566, and 523 connect Thr252 with the Glu366. Water 901 and the alcohol side chain of Thr252 are in hydrogen bond distance with the distal oxygen of the O_2 axial ligand. Hydrogens are not shown for clarity.

protein structure is significant for selectivity, binding affinity, and reaction kinetics and cannot be incorporated to any great degree with conventional quantum chemical techniques. A QM/MM methodology is well suited to addressing this problem with relatively modest computational resources.

We have investigated different QM/MM systems for each catalytic pathway step. The basic structure includes the full protein, obtained from experimental X-ray structures, combined with different QM regions. For the ferric substrate binding, steps **1→2**, the QM region includes the heme group, Cys357, the water molecule (only in **1**), and camphor (only in **2**). For the ferric superoxo protonation, steps **3→5**, the QM region includes the heme group with the oxygen molecule ligand, Cys357, Thr252, and the crystallographic waters 901, 902, 566, and 523. To study the camphor hydroxylation, steps **5→6**, the QM region includes the heme group with the oxygen atom ligand, Cys357, and camphor. The different QM regions can be identified with Figures 1 and 2. The total system consists of approximately 7500 QM/MM atoms, with a maximum of 129 QM atoms. Besides the QM/MM studies, we have built different QM active site models. These reference systems, enabling modeling of the core reactive region in the absence of the protein, are intended to facilitate the assignment of specific structural or energetic effects to the protein.

All crystallographic waters are incorporated into in the QM/MM system. Surface polar amino acids, Lys, Arg, Glu, and Asp, are neutralized if they do not form a salt bridge, which yields a zero net charge of the overall system. Their position is then constrained through the minimization. Such a protocol introduces approximate solvation effects (i.e., screening of ionized groups on the protein surface by high dielectric water) and is justified by the buried nature of the active site. Geometry optimizations are carried out using the B3LYP[33−36] functional in combination with the 6-31G* basis set (basis 1). Iron is represented using an LACVP** basis[37−39] that includes an effective core potential. Several single-point energy calculations are performed using Dunning's[40] correlation consistent triple-ζ basis cc-pVTZ(-f) to recompute the energies (basis 2). All QM calculations have been performed with the Jaguar suite of ab initio electronic structure programs. The QM/MM calculations are carried out with the QSite program,[41] which was

(29) Kamachi, T.; Yoshizawa, K. *J. Am. Chem. Soc.* **2003**, *125* (15), 4652−4661.
(30) Taraphder, S.; Hummer, G. *J. Am. Chem. Soc.* **2003**, *125* (13), 3931−3940.
(31) Egawa, T.; Shimada, H.; Ishimura, Y. *Biochem. Biophys. Res. Commun.* **1994**, *201* (3), 1464−1469.
(32) Newcomb, M.; Aebisher, D.; Shen, R.; Chandrasena, E. P.; Hollenberg, P. F.; Coon, M. J. *J. Am. Chem. Soc.* **2003**, *125* (20), 6064−6065.
(33) Slater, J. C. *Quantum Theory of Molecules and Solids, Vol. 4: The Self-Consistent Field for Molecules and Solids*; McGraw-Hill: New York, 1974.
(34) Becke, A. D. *J. Chem. Phys.* **1993**, *98* (7), 5648−5652.
(35) Lee, C. T.; Yang, W. T.; Parr, R. G. *Phys. Rev. B* **1988**, *37* (2), 785−789.
(36) Vosko, S. H.; Wilk, L.; Nusair, M. *Can. J. Phys.* **1980**, *58* (8), 1200−1211.
(37) Hay, P. J.; Wadt, W. R. *J. Chem. Phys.* **1985**, *82* (1), 270−283.
(38) Wadt, W. R.; Hay, P. J. *J. Chem. Phys.* **1985**, *82* (1), 284−298.
(39) Hay, P. J.; Wadt, W. R. *J. Chem. Phys.* **1985**, *82* (1), 299−310.
(40) Dunning, T. H. *J. Chem. Phys.* **1989**, *90* (2), 1007−1023.
(41) *QSite*; Schrödinger, Inc.: Portland, OR, 2001.

Table 1. QM/MM Optimized and QM Single-Point Energies for the Doublet, Quartet, and Sextet Spin States for the Resting State (**1**) and the Substrate Binding (**2**) Structures[a]

	QM/MM	QM	
	RODFT (Fe/S)	UDFT (Fe/S)	RODFT (Fe/S)
1 doublet	0.0 (0.90/0.04)	0.0 (0.86/0.10)	0.0/**0.0** (0.90/0.10)
1 quartet	9.5 (2.47/0.25)	3.4 (2.49/0.42)	4.6/**4.1** (2.40/0.36)
1 sextet	20.8 (4.09/0.25)	3.5 (3.95/0.42)	4.5 (4.03/0.39)
2 doublet	5.6 (0.88/0.05)	4.3 (0.90/0.08)	2.9/**2.6** (0.85/0.10)
2 quartet	0.0 (2.38/0.30)	0.0 (2.41/0.47)	0.0/**0.0** (2.30/0.43)
2 sextet	2.0 (4.02/0.30)	0.3 (3.92/0.44)	0.2 (4.00/0.38)

[a] QM single-point energies on active site models are at both the RODFT/UDFT methods. The QM model geometries are directly extracted from the QM region of the QM/MM minimized structures. Sulfur and iron spin densities are shown in parentheses. Energies are in kcal/mol. The lowest energy state for each structure is used as the energy origin. In bold numbers, for the QM RODFT system, energy reevaluation of the lowest and highest energy state using basis 2.

developed via a close coupling of Jaguar[42] and the IMPACT[43] protein modeling program of Levy and co-workers. The QM/MM methodology and protocol, as well as extensive validation studies demonstrating excellent agreement with fully QM calculations for peptides and protein active sites, have been described extensively elsewhere.[44,45] These studies suggest that the errors in the QM/MM methodology are typically less than 1−2 kcal/mol, likely a smaller contributor to the error than uncertainties in relative energies obtained with the DFT protocol (estimated for metal containing systems to be on the order of 2−3 kcal/mol).

Results

Substrate Binding. Steps 1→2. Before focusing on the major unknown aspects of the catalytic pathway, steps **3** to **6**, we tested our methodology on the substrate binding step. The resting state and the camphor binding structures have been modeled from 1phc.pdb and 1dz4.pdb, respectively. After neutralization of the system, as described in the methods section, a QM/MM minimization was performed for the doublet, quartet, and sextet spin states for both the resting state **1** and the substrate binding structure **2**. Table 1 shows the optimized energies and relevant spin densities. From each optimized spin state, an active site model has been extracted directly from the QM region (where Cys357 has been modeled by an SCH$_3$ group). These models are used as reference systems to assign specific effects to the protein. Table 1 also shows the energy differences and relevant spin densities for the QM models at the QM/MM geometries. To calibrate the QM/MM RODFT method, the QM model calculations have been performed at both RODFT/UDFT methods (Table 1). Single-point energies, using basis 2, have also been performed for the highest and lowest energies at the RODFT level of theory for the QM systems.

O−O Bond Cleavage. Steps 3→5. To study the redox reaction of the ferric superoxo species (**3** in Figure 1), we have used the recent experimental structure, 1D8Z.pdb. From this experimental structure, we have also derived a ferric superoxo model for the T252A mutant by deleting the hydroxyl group, which is consistent with the mutant X-ray structure (2CP4.pdb) for the substrate binding **2**. As demonstrated by previous

(42) *Jaguar 4.1*; Schrödinger, Inc.: Portland, OR, 2000.
(43) *IMPACT;* Schrödinger, Inc.: Portland, OR, 2000.
(44) Murphy, R. B.; Philipp, D. M.; Friesner, R. A. *J. Comput. Chem.* **2000**, *21* (16), 1442−1457.
(45) Philipp, D. M.; Friesner, R. A. *J. Comput. Chem.* **1999**, *20* (14), 1468−1494.

experimental and theoretical work, a reduction is required prior to the distal oxygen protonation. We proceed by inserting one electron in both the wild type and the T252A mutant QM/MM models. Upon reduction, substantial changes of the hydrogen bond network around the active site are observed. In the wild type, the hydrogen bond distance from W901 and Thr252 to the distal oxygen is reduced by 0.5 and 0.3 Å, respectively, as a result of an increase of electron density at the dioxygen moiety. In the T252A mutant, eliminating the hydroxyl group opens the space for W902 to move toward the heme group. Therefore, we have to equilibrate the structure by running simulated annealing coupled with the QM/MM minimization as described below.

Protonation from W901 does not result in a stable structure. If we build a reaction coordinate for the protonation, where we constrain the proton with a 1.0-Å distance to the distal oxygen as a final point, we obtain a 40-kcal/mol continuously increasing energy profile. Releasing this constraint regenerates the reactant structure in the minimization protocol. Protonation from Thr252, however, is 2.87 kcal/mol exothermic with a 3.9-kcal/mol energy barrier. Figure 3 shows the energy profile and associated core geometries for the wild-type distal oxygen protonation from Thr252. The energy barriers have been estimated with a 0.1 Å increment reaction coordinate. For this initial step, the H−O2 distance at the transition state estimate is 1.4 Å, with the O2−O(Thr252) distance being reduced to 1.61 Å. The proton transferred from the threonine is replaced with an almost negligible barrier (1.0 kcal mol^{-1}, H(W902)−O(Thr252) and O(W902)−O(Thr252) distances being 1.30 Å and 1.47 Å, respectively), by migration of a proton down the water channel that connects the active site with Glu366. Rotation of the new Thr252 proton, to restore the hydrogen bond with the distal oxygen, involves a 2.8-kcal/mol barrier in a 1.2-kcal/mol exothermic process. Although the energy involved in this rotation is not large, it requires a significant readjustment of the water network. A second protonation from the replaced Thr252 proton requires an energy ≥14.0 kcal/mol. We were unable to obtain a stable structure corresponding to a second protonation of the distal oxygen (brackets in Figure 3). Our results, thus, indicate that this last step, cleaving the O−O bond and forming a water molecule, is a concerted step. The 14.0-kcal/mol barrier limit is obtained by constraining the distance between the distal oxygen and the hydrogen involved in the second protonation to 1.05 Å. From this point, an optimization leads to the formation of water and is exothermic by 80 kcal/mol (the minimization was stopped after reaching 1e-04 in an RMS gradient).

The activation energies have been estimated using a reaction coordinate along which the proton is promoted from the reactant to the product state in five intermediate steps. Based on the small observed energy differences, as seen in Figure 3, this reaction coordinate introduces a reasonably quantitative approximation. An analysis of the charge on the transferring hydrogen confirms that a proton is being transferred

Through all the steps shown in Figure 3, single-point calculations of a large QM model of the active site, including a heme model (without the propionate substituients), Thr252, the water channel, and Glu366, did not present any qualitative differences with the QM/MM results and were in quantitative agreement within 2 kcal/mol.
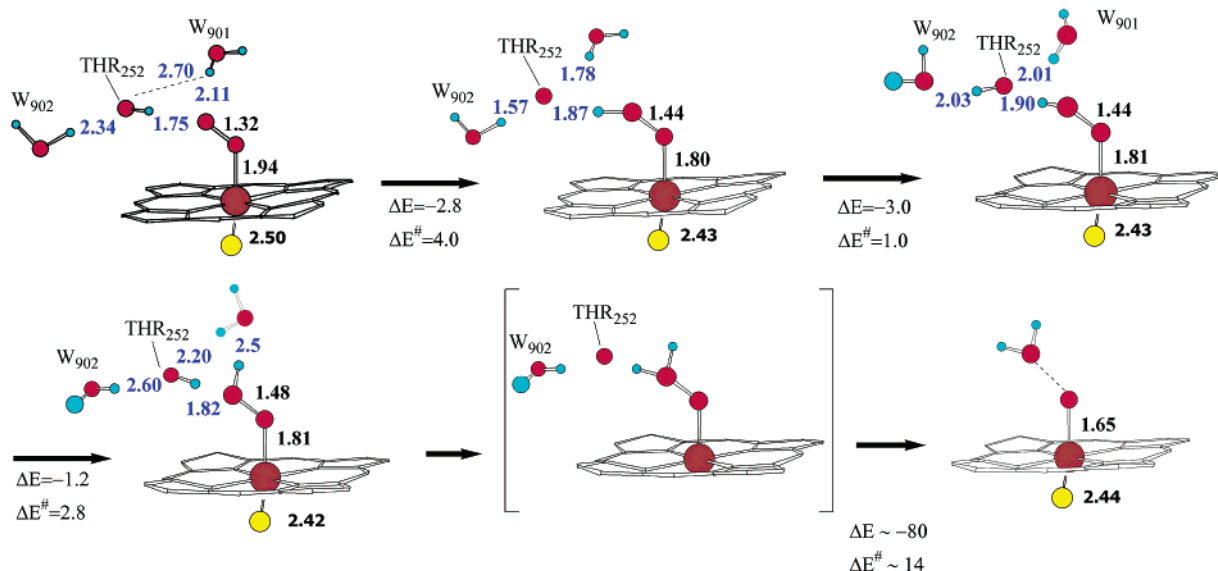
Figure 3. Energies and main geometric distances for the O−O bond cleavage process. Hydrogen bond distances are in blue, and oxygen bond distances, in black. Energies are measured in kcal/mol, and distances in angstroms. Single-point calculations at optimized geometries using basis 2 did not modify the energy differences by more than 1.0 kcal/mol.
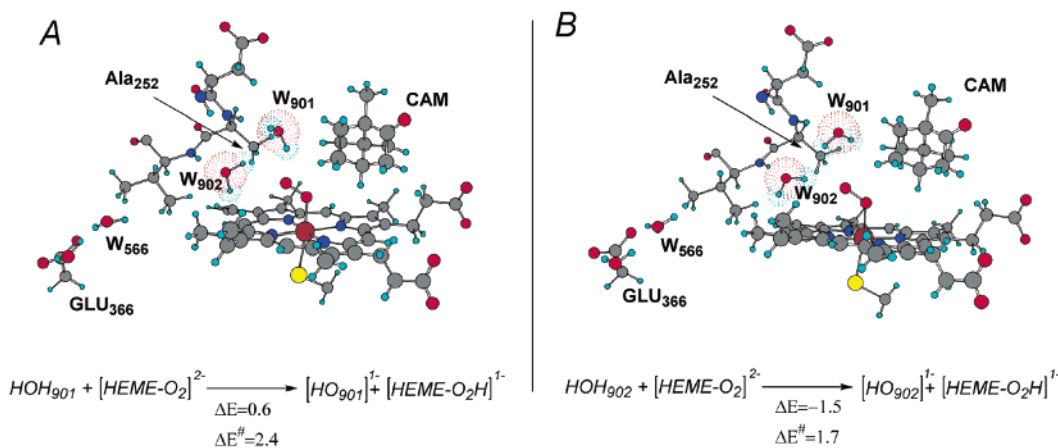

Figure 4. Two different snapshots during the annealing molecular dynamics simulation of the T252A mutant. At the bottom of each panel, main energies involved in the proton transfer from the water directly hydrogen bonding the distal oxygen.

The role of the Thr252 mutation has been studied through an annealing protocol of the MM region. Starting from the minimized reduced ferric superoxo, we freeze a QM region consisting in the heme unit and the Cys357 side chain. The remainder of the protein is then treated as the MM region and is slowly heated to 300 K in six stages of 2 ps. From the 20 trajectories analyzed, the results clearly indicate a breaking of the water channel. In approximately 50% of the trajectories, W902 loses its hydrogen bond interaction with W566 and moves closer to the heme group, establishing a close interaction with the dioxygen ligand. In the other half of the trajectories, W902 recoils back and forms a strong interaction with W566, losing its connection with the heme unit. When the same annealing procedure is performed with the wild type, the water channel remains stable at all times. Figure 4 shows two different snapshots during the T252A mutant annealing simulations, in which a close interaction of both W901 and W902 with the heme unit can be observed. In panel A, W901 directly hydrogen bonds to the distal oxygen while W902 is involved in a hydrogen bond with W901. In panel B this role is inverted and W902 now directly hydrogen bonds to the distal oxygen. In both cases,

the network connecting W902 with W566 is broken. Figure 4 also shows the reactant and product relative energies and an estimate for the energy barrier for a protonation reaction from the water hydrogen bonding to the distal oxygen. These energies were obtained from a reduced QM model involving the heme group, W901, W902, Ala252, and an SCH_3 group as a cysteine mimic. The coordinates were directly extracted from the QM/MM annealing trajectory, and only the water hydrogens, the oxygen ligand, the Fe, and the S were allowed to move during the minimization. The transition state energy estimate was obtained from a minimization, where the transferring hydrogen was constrained at half distance between the reactant and the product.

Camphor Hydroxylation. Steps 3→6. Table 2 shows the QM/MM energy profile, spin densities, and geometries along the camphor hydrogen atom abstraction reaction path, focusing only on the reactive core. For this catalytic step, we have focused on the quartet spin state, for which lower abstraction barriers have been observed.[46] The starting coordinates have been

(46) Yoshizawa, K. *J. Organomet. Chem.* **2001**, *635* (1−2), 100−109.

Table 2. Energies, Spin Densities, and Main Distances for the Reactant (RE), Transition State (TS), and Product (PR) along the Hydrogen Abstraction Reaction[a]
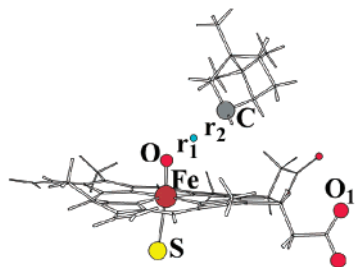
		spin density						distance			
	E	Fe	O	C	S	O_1	Por	r_1	r_2	Fe–O	Fe–S
RE	0.0	1.20	0.70	0.0	0.07	0.20	0.70	2.06	1.09	1.65	2.44
TS	11.7	0.92	0.45	0.52	0.08	0.10	0.81	1.20	1.38	1.75	2.41
PR	4.5	0.86	0.13	0.92	0.06	0.12	0.79	0.97	2.10	1.81	2.39

[a] Energies are in kcal/mol, and distances, in angstroms.

obtained from the recent experimental putative oxo complex, 1DZ9.pdb. The relative reactant/product energy difference, on the order of 24 kcal/mol endothermic in the prior QM model studies cited above, is reduced to 4.5 kcal/mol. The activation barrier is now only 11.7 kcal/mol. If we estimate the zero-point contribution to the barrier as being comparable to the value we have obtained for an MMO model system, on the order of 3.5 kcal/mol, the free energy of the barrier reduces to 8.2 kcal/mol. In using the MMO zero-point result to estimate the zero-point energy for P450, we are making the assumption that this quantum correction is dominated by the mode associated with the C–H–O degrees of freedom, very similar in both systems. Single-point calculations at optimized geometries of the reactants, products, and transition state using basis 2 affect the results by less than 8%. The main difference of the QM/MM spin density analysis with prior QM model studies is the nature of the third unpaired electron (the first two being located in the Fe–O atoms). In particular, we observe some radical character in one of the carboxylic oxygens of the heme that will play a key role in the overall hydroxylation process as discussed below.

The distances, charges, spin densities, and energies of the main atoms involved in the abstraction reaction are similar to those obtained in the analogous ethane hydroxylation by MMO. Also in qualitative agreement with the MMO results is the rotation of the transferred hydrogen out of the C···O–Fe plane, which opens the oxygen for a C–O recombination. Due to the computational cost of the QM/MM calculations, the analysis of the rotation has been less extensive than that in our previous MMO study.[9] Our study has been limited to two different constrained C(camphor)–O(oxo ligand) distances, 2.6 and 2.3 Å. As in the MMO study, the results clearly indicate a large dependence of the rotation on the C–O distance. Rotation of the hydrogen involves 5.6- and 6.0-kcal/mol energy barriers for the 2.6- and 2.3-Å C–O distances. The rotated product is 4.6 kcal/mol endothermic at a 2.6-Å distance but is largely exothermic, 14 kcal/mol, for the 2.3-Å C–O distance. An interpolation of these results indicates that, for a C–O distance of the order of the hydrogen abstraction transition state, the rotation becomes exothermic and requires less energy than the barrier of the abstraction process. Interestingly, the carboxylic

heme oxygen does not present any spin density for the rotated product at both C–O distances (0.12 before the rotation as seen in Table 2).

There is no stable rotamer when releasing the C–O distance constraint. The system spontaneously minimizes into a camphor hydroxylated species in an ∼60-kcal/mol downhill process (the minimization was stopped after reaching 1e-04 in an RMS gradient), breaking the Fe–O bond irreversibly. When the minimization is started from the 2.6-Å C–O distance, however, the system spends several optimization cycles (20 approximately) in a low gradient region (∼2.0e-03 RMS) around the initial structure before it finds an effective downhill path. This optimization indicates the existence of a metastable rotamer at large C–O distances, with a lifetime that might be strongly coupled to the radical substrate stretching.

Discussion

Substrate Binding. Steps 1→2. The results for the doublet, quartet, and sextet spin states for the resting state clearly indicate the role of the protein. Both the QM/MM system and the QM model reproduce the low-spin experimental results.[1] The energy difference between the low- and high-spin states, however, changes considerably when considering the protein. The main source for the low-spin stabilization agrees qualitatively with previous theoretical studies,[22] where a reduced active site model was used. Antibonding interactions of the Fe with the axial ligands (Cys357 and H_2O) stabilize the doublet with respect to the quartet and sextet states. For example, such an interaction translates into a larger Fe–$O(H_2O)$ distance for the optimized QM/MM structures, 2.10 and 2.46 Å in the doublet and sextet states, respectively. In absence of the protein, these optimized distances are 2.18 and 2.65 Å (these distances have been obtained with a reduced QM model as the one used in ref 22). There is, therefore, a larger repulsive steric interaction between the protein active site pocket (residues in close proximity to the water) and the water axial ligand in the high-spin state.

When camphor binds, it displaces the axial ligand and eliminates the antibonding interactions between the Fe and the water, as well as the steric interactions between the water and the active site pocket. For this second structure along the enzymatic cycle, both QM/MM and the QM methods produce very similar results. We observe a clear inversion of the spin state, in perfect agreement with experimental observations. The slightly larger stabilization of the QM/MM high-spin state, when comparing both QM/MM and QM RODFT results, could be explained by electrostatic interactions of the protein with the cysteine sulfur decreasing the spin density in the sulfur atom for all the spin states. Such effect is caused by hydrogen bonds from Gly359 and Leu358 to the sulfur. Therefore high-spin states, with a larger component of Fe–S antibonding interaction, would experience a larger stabilization. In particular, we observe a larger sulfur spin component decrease in the quartet spin states. A more detailed study of the orbital levels for the different catalytic structures, ongoing in our laboratory, supports this initial qualitative analysis.

The overall results for this first catalytic step indicate an active role of the protein in regulating the low–high-spin energy gap, which is essential in the first electron transfer preceding the molecular oxygen binding. The results for the QM subsystem demonstrate a good description of the system with RODFT as well as the use of the basis set 1.

O−O Bond Cleavage. Steps 3→5. Our calculations demonstrate that the first proton must come from Thr252 through a 3.9-kcal/mol barrier with an overall thermodynamic driving force of −3.0 kcal/mol. Protonation from W901 is energetically unfavorable. The main differential element between both proton donors is the stabilization of the negative oxygen atom that remains after the proton is transferred. Water 901 and 902 are ideally positioned to assist the Thr252 after protonation. These results are consistent with previous studies on P450eryf,[24] where the role of a water network is crucial for the distal oxygen protonation. The proton transferred from the threonine is replaced with an almost negligible barrier (1.0 kcal/mol), by migration of a proton down the water channel that connects the active site with Glu366. This second energy profile indicates that both transfers, from Thr252 to the distal oxygen and from W902 to Thr252, might happen in a concerted step. This constitutes an important structural feature differentiating between proton donation by Thr252 and W901 for this second protonation step. To establish a similar mechanism for W901, we would need to redirect Thr252 to force a hydrogen bond with W901. Such a move would involve a large reorganization in the active site and would break the Thr252−O_2 hydrogen bond, which, after the reduction of **3**, appears to be a very strong interaction.

The Thr252 new hydrogen rotation and the second proton transfer to the distal oxygen both involve a major hydrogen bond rearrangement and a relatively large proton-transfer barrier. These processes will require several picoseconds, which translates into a stabilization of the single proton product **4**, which would account for the recently observed EPR signal of an "H-bonded ferric hydroperoxo" species.[13]

Our results are consistent with isotopic labeling studies, where the proximal oxygen is transferred to substrates, while the distal oxygen is involved in the concurrent formation of water.[25,26] One question arises from this mechanism: the ultimate source of protons. The water channel connects Thr252 with Glu366. However, mutations of Glu366 do not affect the enzymatic reaction. It is therefore necessary to study the protein response to the first distal oxygen protonation, possibly involving major conformational changes. Present work in our laboratory is trying to address this question.

Protonation of the distal oxygen in the T252A mutant is energetically favorable. As observed in Figure 4, both W901 and W902 might now be involved as proton donors. There is, however, a clear breaking of the water channel and, as a consequence, a disruption of further proton delivery to the active site. Along the annealing simulation, the water−O_2 interaction is now less selective. For example, water 902 exhibits a larger mobility than the alcohol group in Thr252, which is largely constrained by the protein structure. This combination of factors, the disruption of the water network and the high mobility of both waters, increases the possibilities of an enhancement of the yield of a decoupling channel. In particular, the presence of the two waters is consistent with the net reaction for hydrogen peroxide production, $2H_2O + O_2 \rightarrow 2H_2O_2$, and is in agreement with experimental results. Thus, mutation of Thr252 opens a path for a direct nonselective interaction of the W901 and W902 channel with the dioxygen ligand. In the mutated species, both waters might now assist each other, as shown in Figure 4. Large changes in protonation energies, when adding a second water in very similar environments, have been already reported

previously.[24] The alcohol group of the threonine plays an active role in the enzymatic cycle, not only for the purpose of proton delivery, but also because of its specific interaction with the distal oxygen, which, in absence of Thr252, has a larger autonomy to reorient itself with the different water configurations.

Mutation of the Thr252 hydroxy group with a methoxy group[28] might block the access of water 902 to the active site. The enzyme, however, retains monooxygenase activity with a considerable decrease of O_2 consumption rate. Thus, an alternative path involving a second oxidant could be responsible of the monooxygenase retained activity, in agreement with the Newcomb et al. two-oxidant model.[32] The involvement of Asp251 seems less plausible, since its carboxylic side chain is involved in a strong salt bridge with Arg186. We have performed multiple Asp251 side chains sampling along a molecular dynamics trajectory without obtaining any significant large motion of Asp 251 leading to a rupture of the salt bridge. The side chain sampling method, recently developed in our lab, incorporates an all-atom force field (OPLS-AA) associated with a continuum solvation model employing the surface Generalized Born (SGB) methodology that we have developed several years ago. Hence it represents an improvement in respect to previous Asp251 sampling results where electrostatic terms were neglected.[30] The strength of this Asp-Arg salt bridge does not favor a protonation of Asp251 as proposed recently.[29]

Camphor Hydroxylation. Steps 5→6. Our QM/MM study reveals that the failure to observe compound I in the EPR study is due to the rapid reaction of this intermediate with camphor. Compared with previous reduced theoretical models, the energy profile for the H-atom abstraction changes drastically when the full system is included, as illustrated in Table 2. The energy barrier is exceptionally small and would permit rapid formation of the hydroxylated product from the ferryl intermediate. Furthermore, molecular dynamics studies in progress in our laboratory indicate that the Fe−O stretching mode is activated after the O−O cleavage described above, shortening the camphor−O distance, which promotes the H abstraction reaction.

The critical question, then, is how the enzyme manages to achieve such a low reaction barrier. The main component of this stabilization is based on an electrostatic interaction between the heme carboxylate substituents and the positive residues in close contact with them. Figure 5 summarizes the mechanism, which has been described in detail elsewhere.[47] Compound I can be envisioned as the product of an intramolecular single-electron transfer reaction from the porphyrin ligand to a putative Fe(V) center, to give the Fe(IV) moiety and a radicaloid porphyrin ligand. In this environment, the carboxylate is not strong enough to maintain fully occupied lone pair orbitals on its oxygen atoms, giving rise to the excess spin polarization of 0.2 on one of the two O-atoms.[48] Upon hydrogen transfer and electron injection, the first step in Figure 5, the carboxylate ligand removes 0.08 electron units and becomes more negative

(47) Guallar, V.; Baik, M.; Lippard, S. J.; Friesner, R. A. *Proc. Natl. Acad. Sci. U.S.A.* **2003**, *100* (12), 6998−7002.
(48) While correcting the proofs, a QM/MM study by Shaik et al. (*J. Am. Chem. Soc.* **2004**, *126*, 4017−4034) has questioned the role of the heme carboxylic groups in the hydrogen abstraction. Work in progress in our lab further confirms our initial results (manuscript in preparation). We are also working with Prof. Shaik and Prof. Thiel to address the different results observed by the two groups.
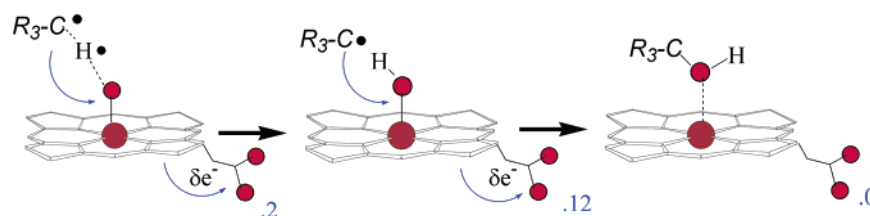
Figure 5. Electron transfer scheme for the hydrogen atom abstraction and hydrogen rotation in the hydroxylation process. Blue numbers show the spin densities of the heme carboxylate oxygen.

by 0.06 units. This additional negative charge interacts favorably with the positively charged Arg299, in hydrogen bond distance with the carboxylate, and translates into a differential electrostatic stabilization. The same process is observed upon the hydrogen rotation, the second step in Figure 5, where a second electron injection into the heme core entirely restores the electronic charge of the carboxylate oxygens. Therefore, the presence of positive residues in the vicinity of the active site stabilizes both the hydrogen abstraction and rotation products (as well as the barriers), leading to an open channel for the substrate's carbon second oxidation and the C−O recombination. The existence of a metastable rotamer, as indicated when releasing the C−O constrain in the rotated product, might explain different experimental EPR and ENDOR signals[13] after the hydrogen abstraction process.

Conclusion

We have produced the first exhaustive theoretical study of the hydroxylation catalytic pathway of cytochrome P450cam by means of a mixed quantum mechanics/molecular mechanics (QM/MM) technique. Our results describe an important role of the protein in several steps of the enzymatic cycle. In the binding process, the protein controls the energy gap between the high- and low-spin state, which is a key factor in the reduction potential of the heme group. In the distal oxygen protonation of the ferric superoxo species, Thr252 has an active and selective role in the delivery of protons. Such a protonation mechanism is only possible with the support of a water channel. Finally, the protein environment of the active site plays a central role in the reactivity of the active species, compound I.

The models developed here find explanation for most of the controversal experimental data in the wild type and the Thr252 to Ala mutant. They can be used to obtain further detailed comparisons with experimental results and to suggest new experiments with this and other proteins that employ protoporphyrin IX, as well as enabling predictions for active site mutations of the enzyme.